

Open-Vocabulary Segmentation with Unpaired Mask-Text Supervision

Zhaqing Wang^{1,4} Xiaobo Xia¹ Ziye Chen² Xiao He⁴ Yandong Guo⁴
 Mingming Gong^{2,3} Tongliang Liu¹

¹The University of Sydney ²The University of Melbourne

³Mohamed bin Zayed University of Artificial Intelligence ⁴AI2Robotics

<https://github.com/DerrickWang005/Uni-OVSeg.pytorch>

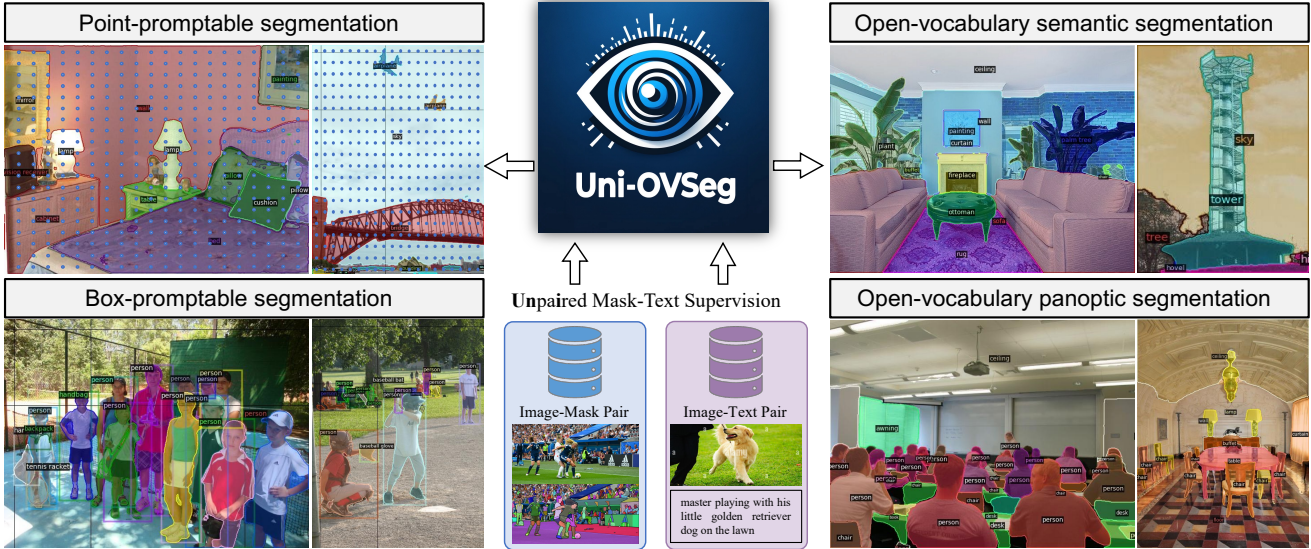


Figure 1. The proposed Uni-OVSeg framework learns **open-vocabulary segmentation** with **unpaired mask-text supervision**. Compared to the labour-intensive image-mask-text annotations, independent image-mask and image-text pairs are easier to collect. With one suite of weights, given different visual prompts (e.g., points and boxes), Uni-OVSeg can segment and categorise various objects and stuff from an open set of vocabulary in the real world.

Abstract

Contemporary cutting-edge open-vocabulary segmentation approaches commonly rely on image-mask-text triplets, yet this restricted annotation is labour-intensive and encounters scalability hurdles in complex real-world scenarios. Although some methods are proposed to reduce the annotation cost with only text supervision, the incompleteness of supervision severely limits the versatility and performance. In this paper, we liberate the strict correspondence between masks and texts by using independent image-mask and image-text pairs, which can be easily collected respectively. With this unpaired mask-text supervision, we propose a new weakly-supervised open-vocabulary segmentation framework (Uni-OVSeg) that leverages confident pairs of mask predictions and entities in text descriptions. Using the independent image-mask and image-text pairs, we predict a set of binary masks and associate them with entities

by resorting to the CLIP embedding space. However, the inherent noise in the correspondence between masks and entities poses a significant challenge when obtaining reliable pairs. In light of this, we advocate using the large vision-language model (LVLM) to refine text descriptions and devise a multi-scale ensemble to stabilise the matching between masks and entities. Compared to text-only weakly-supervised methods, our Uni-OVSeg achieves substantial improvements of 15.5% mIoU on the ADE20K datasets, and even surpasses fully-supervised methods on the challenging PASCAL Context-459 dataset.

1. Introduction

Open-vocabulary segmentation refers to the segmentation and categorisation of objects from an expansive and unrestricted vocabulary, even though the object categories within the vocabulary are not encountered during train-

ing [16, 35, 70]. Compared to traditional closed-vocabulary segmentation [13, 83], which depends on predefined training categories and cannot recognise absent categories, open-vocabulary segmentation can segment any category with arbitrary text descriptions. This innovative segmentation paradigm has garnered considerable attention [39, 67] and opened up numerous potential applications [72, 87, 88].

Cutting-edge approaches in open-vocabulary segmentation typically leverage supervision with triplet annotations that are composed of images, masks, and corresponding texts [63, 76]. It is worth noting that strict alignment between each mask and text results in an expensive annotation cost. To mitigate this, some weakly-supervised methods propose using only text supervision [6, 64, 65]. However, learning with this supervision, the model falls short in capturing complex spatial details, which is suboptimal for dense prediction. Furthermore, this type of supervision lacks positional information, making the model difficult to distinguish different instances with the same semantic class. These issues severely limit the versatility and segmentation performance of existing weakly-supervised methods.

Motivated by that, in this paper, we propose an advanced weakly-supervised open-vocabulary segmentation framework, named Uni-OVSeg, to reduce the annotation expense while significantly enhancing performance. In essence, we liberate the strict correspondence between masks and texts, by using independent image-mask and image-text pairs. These two types of pairs can be easily collected from different sources, as illustrated in Fig. 1, such as SA-1B [34] for image-mask pairs and CC3M [50] for image-text pairs. By resorting to independent image-mask and image-text pairs, our Uni-OVSeg has a strong segmentation ability to group semantically similar pixels, and align mask-wise embeddings with entity embeddings of texts into the same space, achieving open-vocabulary segmentation.

Technically, when presented with an image-mask pair, we train a visual prompt encoder, a pixel decoder, and a mask decoder to generate a set of binary masks. The collected image-text pair often contains certain texts that does not match the image [52], leading to an incorrect correspondence between masks and entities. We employ the LLaVa model [42] to refine the quality of text descriptions, coupled with a ChatGPT-based parser for precise entity extraction. For mask-text alignment, we introduce a mask-text bipartite matching to exploit confident pairs of predicted masks and entities. A multi-scale feature adapter is designed to enhance the visual embeddings of predicted masks, which are further aligned with the text embeddings of corresponding entities. As masks and text are allowed to be unpaired in Uni-OVSeg, a multi-scale ensemble is introduced to improve the quality of visual embeddings and tackle inherent noise in the correspondence between masks and entities effectively, thereby stabilising the matching process. During

the inference phase, a zero-shot classifier, built by embedding target dataset category names, assigns categories to predicted masks, enabling the system to segment objects across an open vocabulary. We summarise our contributions in the following aspects:

1. We introduce a new framework Uni-OVSeg and offer an innovative solution that significantly reduces the need for costly triplet annotations. This makes open-vocabulary segmentation more accessible and scalable.
2. Uni-OVSeg employs a visual prompt encoder, pixel decoder, and mask decoder for binary mask segmentation. An inclusion of refinement of text descriptions, multi-scale ensemble enhances segmentation performance by alleviating inherent noise in mask-text correspondence.
3. With one suit of weights, we achieve 32.6% mIoU on the ADE20K dataset, and even surpassing the state-of-the-art FC-CLIP [76] on the challenging PASCAL Context-459 dataset. Comprehensive ablation studies and discussions are also provided.

2. Related works

Generic segmentation. Given an image, segmentation of specific visual concepts has remained an ongoing research topic in computer vision, as indicated by the extensive literature on it [23, 33, 44]. Generic segmentation mainly includes semantic segmentation [12, 44, 77, 79], instance segmentation [4, 7, 23], and panoptic segmentation [11, 11, 33, 56], related to different levels of granularity. In more detail, semantic segmentation [12, 20, 28, 38, 78] aims to assign a label to each pixel of the input image, according to their respective semantic classes. In addition, instance segmentation [53, 54, 59] attempts to distinguish different object instances of the same semantic class. Panoptic segmentation [9, 57, 74, 75] combines the characteristics of semantic segmentation and instance segmentation. Following a close-vocabulary assumption, previous works only can predict a predefined set of object categories. In this paper, we aim to build an advanced open-vocabulary segmentation system, which can categorise objects and stuff from an open set of vocabulary in the real world.

Vision foundation models. Recent advancements in visual foundation models have diversified optimisation techniques across various learning paradigms. These developments range from vision-only pretraining [2, 24, 25, 61, 62] to joint vision-language pre-training [30, 48, 73], and extend to multi-modal frameworks that integrate visual prompting [1]. A prime example of this evolution is SAM [34], which shows the potential of extensive training for general segmentation, offering impressive generalisability and scalability. Despite its impressive capabilities, SAM cannot categorise predicted masks into different semantic classes, which is limited by the supervision of the image-mask pairs.

More recently, Semantic-SAM [36] unifies different sources of human-annotated segmentation datasets and augments SAM by adding semantic labels and increased levels of granularity. In our work, our aim is to develop a more flexible vision foundation model, which can be trained with unpaired mask-text supervision (*e.g.*, independent image-mask and image-text pairs) and can be easily adapted to different segmentation tasks.

Open-vocabulary segmentation. Open-vocabulary segmentation counters the constraints of closed-vocabulary segmentation by allowing the segmentation of a diverse range of classes, even those unseen during training [21, 67, 68, 80]. Existing works [17, 66, 76] leverage the pretrained vision-language models (*e.g.*, CLIP [48] and ALIGN [30]) to perform open-vocabulary segmentation. Most open-vocabulary segmentation methods commonly utilise human-annotated supervision (*i.e.*, the image-mask-text triplets) to generalise the capability of vision-language models from the image level to the pixel level. To reduce the dependency on this labour-intensive supervision, some weakly-supervised methods are proposed to use only text supervisions [46, 65]. They learn to group image regions into shaped segments, but struggle to distinguish different instances with the same semantic class and the segmentation performance is unsatisfactory [64, 85]. This dilemma drives our pursuit of more advanced open-vocabulary segmentation framework, where the aim is to enjoy as low annotation cost as possible and simultaneously achieve significant performance.

3. Method

In this section, we first define the problem of open-vocabulary segmentation in Sec. 3.1. We then introduce a straightforward baseline in Sec. 3.2. Finally, we present our proposed Uni-OVSeg framework in Sec. 3.3, including an overview, mask generation, mask-text alignment, and open-vocabulary inference.

3.1. Problem definition

Given an image $\mathbf{I} \in \mathbb{R}^{H \times W \times 3}$, where H and W denote the height and width of the image respectively, open-vocabulary segmentation aims to segment the image into a set of masks with associated semantic classes:

$$\{\mathbf{y}_i\}_{i=1}^k = \{(\mathbf{m}_i, \mathbf{c}_i)\}_{i=1}^k. \quad (1)$$

The k masks $\mathbf{m}_i \in \{0, 1\}^{H \times W}$ include the associated ground truth class \mathbf{c}_i [76]. Unlike traditional image segmentation tasks [23, 33, 44], open-vocabulary segmentation is more challenging because inference classes are not observed during training. During the evaluation, the test categories \mathbf{C}_{test} are different from $\mathbf{C}_{\text{train}}$, which contain novel

categories not seen in training, *i.e.*, $\mathbf{C}_{\text{train}} \neq \mathbf{C}_{\text{test}}$. Different from previous works [64, 66], in our setting, no paired human-annotated mask and semantic category is provided in advance for any training image. We assume that the category names of \mathbf{C}_{test} are available, which are represented in the form of natural language.

3.2. Baseline

We introduce a straightforward baseline using the knowledge of image-text and image-mask pairs. Specifically, we employ a CLIP model as the visual and text encoder, which is trained on a large amount of image-text pairs. Afterward, we use the image-mask pairs to obtain a branch of mask generation, predicting a set of binary masks. To perform open-vocabulary segmentation, we crop and pool the CLIP image features based on these predicted masks, which are further classified by the CLIP text embeddings. Although this straightforward baseline enables open-vocabulary segmentation, it exhibits an obvious knowledge gap between the image-level and pixel-level tasks.

3.3. Uni-OVSeg framework

Overview. An overview of our framework Uni-OVSeg, for weakly-supervised open-vocabulary segmentation is illustrated in Fig. 2. On a macro level, Uni-OVSeg contains a CLIP model to extract features of both images and text descriptions. With the image-mask pairs, a branch of mask generation, including a visual prompt encoder, a pixel decoder and a mask decoder, is employed to predict a set of binary masks of an input image. With the image-text pairs, mask-text bipartite matching is used to exploit confident pairs between predicted masks and entities in text descriptions. Afterward, we adopt a multi-scale feature adapter to enhance the mask-wise visual embeddings, which are further aligned with associated entity embeddings based on the confident pairs. Finally, we perform open-vocabulary segmentation with the above-mentioned parts. More details can be found in Appendix A.

Mask generation. Given an input image \mathbf{I} , mask generation aims to predict a set of binary masks \mathbf{m} . These masks represent groups of semantically similar pixels on various locations of the image. To effectively associate these masks with visual prompts (*e.g.*, points and boxes), we adopt an architecture inspired by [13, 34], employing a visual prompt encoder, a pixel decoder and a query-based mask decoder. Both point (x, y) and box (x, y, w, h) prompts are transformed into unified anchor boxes. Each point is converted into an anchor box with a predefined width $w' = 4$ and height $h' = 4$, effectively approximating the location of points. To address the challenge of predicting masks with varying granularities, as depicted in Fig. 2, we encode each point into two positional embeddings $\mathbf{q}_n^{\text{loc}} \in \mathbb{R}^{2 \times \text{dim}}$ using sine encoding [55], and combine them with M distinct

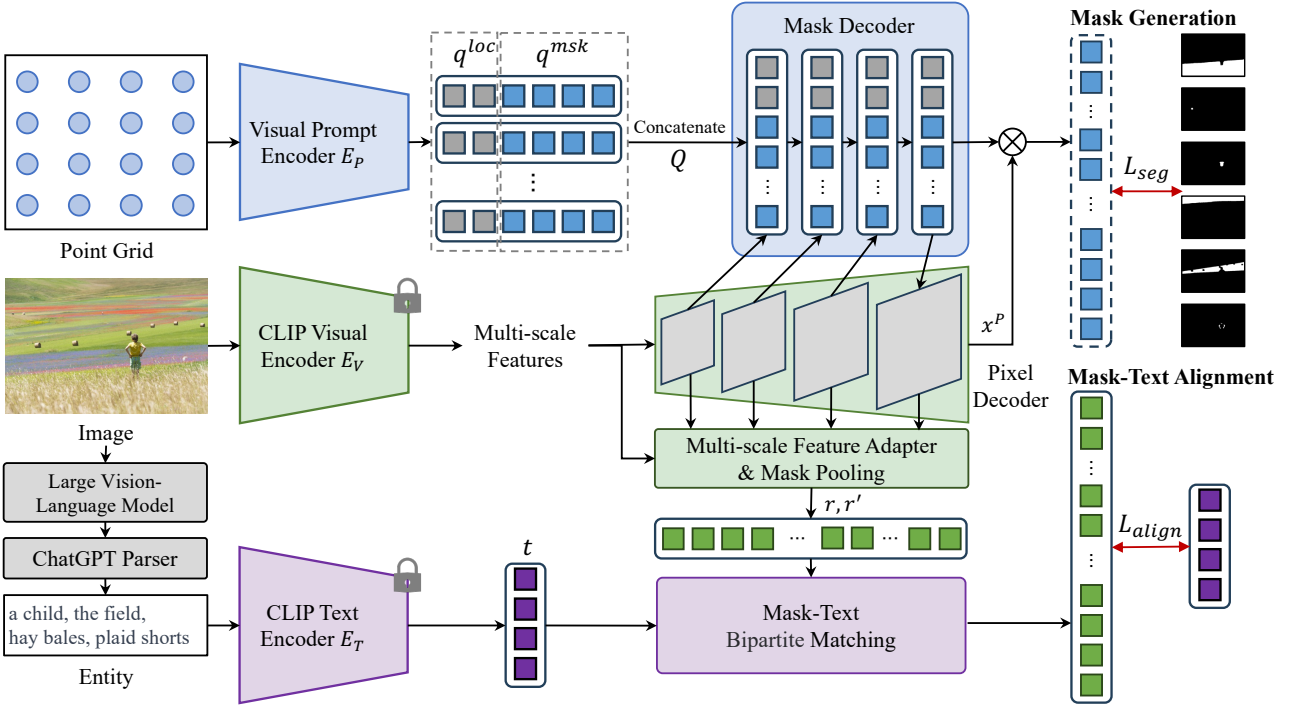


Figure 2. **Overview of the Uni-OVSeg framework.** This framework consists of feature extraction, mask generation, and mask-text alignment. A frozen CLIP model and prompt encoder are used for image and text feature extraction and prompt encoding, respectively. We employ a mask and pixel decoder for binary mask prediction. A mask-text bipartite matching is designed to exploit confident mask-entity pairs. Visual prompts using boxes are omitted for simplicity.

mask embeddings $\mathbf{q}^{msk} \in \mathbb{R}^{M \times dim}$. Each mask embedding is a learnable vector corresponding to a specific granularity level. For box prompts, the process involves encoding into two position embeddings followed by concatenation with a singular mask embedding, as each box is linked to a unique object. Afterward, we represent N input location prompts as a set of query embeddings $\mathbf{Q} = \mathbf{q}_1, \dots, \mathbf{q}_N$. For the i -th query,

$$\mathbf{q}_i = \text{Concat}(\mathbf{q}_i^{loc}; \mathbf{q}_i^{msk}) + \mathbf{q}_i^{type} + \mathbf{q}_i^{feat}, \quad (2)$$

where $\mathbf{q}_i^{type} \in \mathbb{R}^{dim}$ denotes the query type, chosen from either the point or the box. $\mathbf{q}_i^{feat} \in \mathbb{R}^{dim}$ is the content embedding sampled from visual features. For box prompts, we sample visual features based on the center of each box.

Subsequently, to capture the multi-scale information, a pixel decoder equipped with multi-scale deformable attention [86] is used and outputs enhanced pixel features \mathbf{x}^p . These features, in conjunction with the query embeddings, are fed into the query-based mask decoder to predict binary masks. Each layer of the mask decoder comprises a masked cross-attention mechanism [13], a self-attention layer [55], and a feed-forward network. The binary masks for each visual prompt \mathbf{m}_n are derived through a matrix multiplication between the query embeddings and pixel features,

$$\mathbf{m}_n = \text{Sigmoid}(\mathbf{q}_n^{msk} \cdot \mathbf{x}^p), \quad (3)$$

where $\mathbf{m}_n \in \mathbb{R}^{M \times H \times W}$ and $\text{Sigmoid}(\cdot)$ is the sigmoid function to normalize the mask values into $[0, 1]$. An input point is likely to exist in different granularity masks simultaneously. To capture this property and accurately predict multi-granularity masks, unlike SAM [34], we devise a many-to-many matching strategy to automatically associate the ground-truth masks with the mask predictions of each point, allowing a more comprehensive use of image-mask pairs. Once matching, we compute the segmentation loss for each mask prediction \mathbf{m}_i with the corresponding ground-truth mask \mathbf{y}_j^{msk} ,

$$\mathcal{L}_{seg}(\mathbf{m}_i, \mathbf{y}_j^{msk}) = \lambda_{bce} \cdot \mathcal{L}_{bce}(\mathbf{m}_i, \mathbf{y}_j^{msk}) + \lambda_{dice} \cdot \mathcal{L}_{dice}(\mathbf{m}_i, \mathbf{y}_j^{msk}), \quad (4)$$

where λ_{bce} and λ_{dice} are two hyper-parameters to balance the binary cross-entropy loss \mathcal{L}_{bce} and the dice loss \mathcal{L}_{dice} . Note that we apply no penalty to the remaining unmatched mask predictions, ensuring that multiple granularity masks can be predicted for each point.

Mask-text alignment. To enable the model categorising the predicted masks from an open set of vocabulary, given the image-text pairs, we build the correspondence between objects in the image and entities in the text description. Once a set of binary masks \mathbf{m} are generated from the input image, we obtain the region embeddings \mathbf{r}_i by employing a

mask pooling layer P and the CLIP visual projector F_v ,

$$\mathbf{r}_i = F_v(P(\mathbf{x}^v, \mathbf{m}_i)), \quad (5)$$

where \mathbf{x}^v denotes the visual features extracted from the CLIP visual encoder. However, the collected image-text pairs often contain mismatches between visual and textual information. Directly aligning these incorrect correspondence leads to suboptimal segmentation performance. To alleviate that, we adopt a large vision-language model, LLaVa [42], to refine the text descriptions. For each text description, traditional natural language processing tools (such as NLTK) struggle to extract reliable entities due to the complex structure and diversity of natural language. Recently, ChatGPT has demonstrated strong capabilities in contextual processing, thereby more accurately identifying noun phrases. Therefore, we utilise the ChatGPT-based parser to extract reliable entities¹. Afterwards, each entity combined with the prompts used in [22] is fed into the CLIP text encoder to obtain the text embedding t_k . we calculate a cost matrix Δ between the region embeddings and text embeddings,

$$\delta_{i,j} = \frac{\exp(\delta'_{i,j})}{\sum_j \exp(\delta'_{i,j})}, \quad \delta'_{i,k} = 1 - \frac{\mathbf{r}_i \cdot \mathbf{t}_k}{\|\mathbf{r}_i\|_2 \|\mathbf{t}_k\|_2}, \quad (6)$$

where $\delta'_{i,k}$ denotes the reverse cosine similarity between the i -th region embedding and the k -th text embedding. The scale of objects within images often varies significantly. To enhance the quality of matching, we extract region embeddings at different scales by utilising multi-resolution images. This approach allows us to integrate cost matrices from different scales to derive the final cost matrix,

$$\Delta' = \frac{1}{S} \sum_{s=1}^S \Delta_s, \quad (7)$$

where S denotes the number of scales and Δ_s is the cost matrix at the s -th scale. With this matrix, we apply the bipartite matching algorithm [31] to obtain the confident pairs. Finally, we fed the multi-scale visual features and the CLIP visual features into a multi-scale feature adapter to obtain the advanced region embeddings \mathbf{r}'_i , and compute the cosine similarity loss for each paired region and text embedding,

$$\mathcal{L}_{align}(\mathbf{r}'_i, \mathbf{t}_k) = 1 - \frac{\mathbf{r}'_i \cdot \mathbf{t}_k}{\|\mathbf{r}'_i\|_2 \|\mathbf{t}_k\|_2}. \quad (8)$$

Open-vocabulary inference. During inference, given the test categories \mathbf{C}_{test} , we conduct prompt engineering [21] and use the CLIP text encoder to extract text embeddings

for open-vocabulary segmentation. For each input image, we input an uniform point grid as the visual prompt to predict a set of binary masks, and compute the cosine similarity with the text embeddings to predict the category with the maximum similarity as the label of the corresponding mask.

4. Experiments

4.1. Implementation details

Datasets. During training, we randomly sample the 30% subset from the SA-1B dataset [34], which contains ~ 3 million images and ~ 0.3 billion masks. Although this supervision provides diverse binary masks, it lacks the semantic class for each mask. In addition, following Chen et al. [8], we collect about 1.3 million image-text pairs and use a large vision-language model to refine them. Afterward, we use the ChatGPT-based parser to extract entities with descriptive words from these text descriptions.

Training configuration. We adopt the ConvNext-Large CLIP model [43, 48] from OpenCLIP [29]. For mask segmentation training, we mainly follow Cheng et al. [13] and adopt a similar training recipe and losses without any special design. The image input size is 896×896 and the batch size is 56. The model is optimised with AdamW [32, 45] with a learning rate of 1×10^{-4} and a weight decay of 0.05. We train the model for 60k iterations and update the learning rate by a multi-step decay schedule. Besides, we adopt the same training recipe for mask-text alignment. The whole training is conducted on 56 V100-32G for ~ 2.5 days. λ_{bce} and λ_{dice} are set to 2 and 1, respectively.

Evaluation & metrics. We evaluate our model mainly on three tasks, including open-vocabulary semantic segmentation, open-vocabulary panoptic segmentation, and promptable segmentation. Following previous work [76], we adopt prompt engineering from [21, 66] and prompt templates from [22, 37]. For **open-vocabulary semantic segmentation**, we zero-shot evaluate the model on the COCO [40], ADE20K [84], PASCAL [18] datasets. The open-vocabulary semantic segmentation results are evaluated with the mean Intersection-over-Union (mIoU). For **open-vocabulary panoptic segmentation**, we evaluate the model on the COCO, ADE20K, and Cityscapes [15] datasets. We report the panoptic quality (PQ), semantic quality (SQ), and recognition quality (RQ) for open-vocabulary panoptic segmentation. For **promptable segmentation**, we report the 1-Point and 1-Box IoU (Oracle) on a wide range of datasets. Oracle denotes that we select the output mask with the max IoU by calculating the IoU between the prediction and target mask. More details can be found in Appendix B.

¹<https://openai.com/chatgpt>

Table 1. **Open-vocabulary semantic segmentation performance.** We mainly compare with the fully-supervised and weakly-supervised methods. “COCO S.”, “COCO P.” and “COCO C.” denote the COCO stuff, panoptic and caption datasets. “O365” denotes the Object 365 dataset. “M. 41M” denotes the merged 41M image dataset. We report mIoU for all datasets.

Method	Training Data	A-847	PC-459	A-150	PC-59	PAS-21	PAS-20	Citys
		mIoU (%)						
Fully-supervised method (image-text-mask pair)								
SimBaseline [67]	COCO S.	-	-	15.3	-	74.5	-	-
ZegFormer [16]	COCO S.	-	-	16.4	-	73.3	-	-
LSeg+ [35]	COCO S.	3.8	7.8	18.0	46.5	-	-	-
OVSeg [39]	COCO S.	9.0	12.4	29.6	55.7	-	94.5	-
SAN [68]	COCO S.	13.7	17.1	33.3	60.2	-	95.5	-
OpenSeg [21]	COCO P. + C.	6.3	9.0	21.1	42.1	-	-	-
ODISE [66]	COCO P.	11.1	14.5	29.9	57.3	84.6	-	-
X-Decoder [87]	COCO P. + C.	-	-	25.0	-	-	-	47.3
OpenSEED [80]	COCO P. + O365	-	-	22.9	-	-	-	46.1
MaskCLIP [17]	COCO P.	8.2	10.0	23.7	45.9	-	-	-
FC-CLIP [76]	COCO P.	14.8	18.2	34.1	58.4	81.8	95.4	56.2
Weakly-supervised method (image-text pair or image-text & image-mask pair)								
GroupViT [64]	GCC + YFCC	4.3	4.9	10.4	23.4	52.3	79.7	18.5
TCL [6]	GCC	-	-	14.9	30.3	51.2	77.5	23.5
OVSeg [65]	CC4M	-	-	5.6	-	53.8	-	-
SegCLIP [46]	CC3M + COCO C.	-	-	8.7	-	52.6	-	-
CLIPPy [49]	HQITP-134M	-	-	13.5	-	52.2	-	-
MixReorg [5]	CC12M	-	-	10.1	25.4	50.5	-	-
SAM-CLIP [58]	M. 41M	-	-	17.1	29.2	60.6	-	-
Uni-OVSeg (Ours)	30% SA1B + M. 1.3M	13.5	18.5	32.6	50.9	78.9	91.9	39.7

4.2. Main results

Open-vocabulary semantic segmentation. As demonstrated in Tab. 1, our study presents a comprehensive comparison of our Uni-OVSeg against previous works across a range of benchmarks. These include ADE20K (encompassing both 150 and 847 class variants), PASCAL Context (459 and 59 class variants), PASCAL VOC (with 20 and 21 class categories), and Cityscapes. Compared to weakly-supervised methods, Uni-OVSeg exhibits remarkable performance improvements across all evaluated datasets. Specifically, in the more challenging datasets of PASCAL Context-459, Uni-OVSeg not only surpasses its weakly-supervised counterparts but also outperforms the cutting-edge fully-supervised methods, *e.g.*, FC-CLIP. This is indicative of Uni-OVSeg’s superior capability in categorizing a diverse array of semantic classes. Furthermore, in the PASCAL VOC benchmarks (20 and 21 classes), Uni-OVSeg demonstrates a substantial enhancement over state-of-the-art weakly-supervised methods, achieving improvements of 18.3% and 12.2% mIoU, respectively, which demonstrates our Uni-OVSeg captures fine-grained spatial structures. These results elevate the practical applicability of weakly-supervised open-vocabulary segmentation to new heights.

Open-vocabulary panoptic segmentation. For open-vocabulary panoptic segmentation, we zero-shot evaluate our model on the COCO, ADE20K, and Cityscapes datasets, shown in Tab. 2. Existing weakly-supervised methods only use text supervision, which causes a challenge to discriminate different instances with the same semantic class. To the best of our knowledge, we are the first to learn open-vocabulary panoptic segmentation with weak supervision. Compared to unsupervised methods, we obviously outperform U2Seg by 1.9% PQ, 1.5%SQ, and 4.4% RQ on COCO datasets. Unfortunately, our used image-mask pairs contain multiple granularity masks, such as object-wise and part-wise masks, which is different with the panoptic segmentation datasets. This discrepancy leads to a number of false positive results, limiting our performance.

Promptable segmentation. To evaluate the segmentation efficacy of Uni-OVSeg in scenarios involving interactive point and box prompts, we conduct comparative analyses with the SAM-ViT/L model across a range of datasets from diverse domains. For visual prompts, we implement a uniform 20×20 point grid as the interactive point prompt and utilise the actual bounding boxes as box prompts. The segmentation performance is measured using the 1-pt IoU (Oracle) metric across all datasets. The results, as demonstrated in Fig. 3, indicate that Uni-OVSeg exceeds SAM in most

Table 2. **Open-vocabulary panoptic segmentation performance.** We mainly compare with the fully-supervised and unsupervised methods. “COCO P.” denotes the COCO panoptic datasets. “COCO” denotes the COCO image dataset. “IN 1K” denotes the ImageNet-1K image dataset. We report PQ, SQ and RQ for all datasets.

Method	Training Data	COCO			ADE20K			Cityscapes		
		PQ	SQ	RQ	PQ	SQ	RQ	PQ	SQ	RQ
Fully-supervised method (image-text-mask pair)										
MaskCLIP [17]	COCO P.	30.9	-	-	15.1	70.5	19.2	-	-	-
ODISE [66]	COCO P.	55.4	-	-	22.6	-	-	23.9	75.3	29.0
FC-CLIP [76]	COCO P.	54.4	83.0	64.8	26.8	71.6	32.3	44.0	75.4	53.6
OPSNet [10]	COCO P.	57.9	84.1	68.2	19.0	52.4	23.0	41.5	67.5	50.0
Unsupervised method (Unlabelled image)										
CutLER+STEGO [60]	IN 1K + COCO	12.4	64.9	15.5	-	-	-	12.4	36.1	15.2
U2Seg [47]	IN 1K + COCO	16.1	71.1	19.9	-	-	-	17.6	52.7	21.7
Weakly-supervised method (image-text & image-mask pair)										
Uni-OVSeg (Ours)	30% SA1B + M. 1.3M	18.0	72.6	24.3	14.1	66.1	19.0	17.5	65.2	23.5

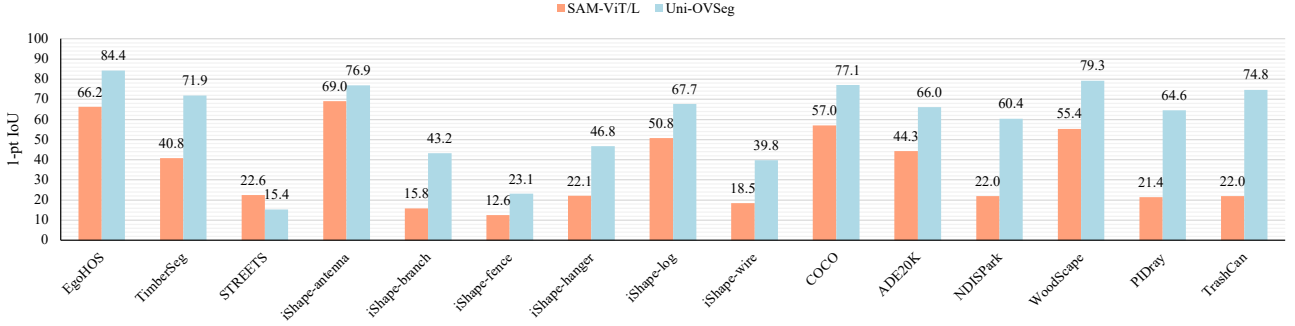


Figure 3. **Point-promptable segmentation performance.** We compare our method with SAM-ViT/L [34] on a wide range of datasets. Given a 20×20 point grid as visual prompt, we select the output masks with max IoU by calculating the IoU with the ground-truth masks. We report 1-pt IoU for all datasets.

datasets when employing point and box prompts. In particular, Uni-OVSeg significantly surpasses SAM in terms of IoU by 31.1%, 20.1%, and 43.2% on the TimberSeg, COCO instance, and PIDray datasets, respectively. Additionally, we provide a visualisation of the segmentation results of both SAM and Uni-OVSeg in Fig. 4. The visualisation reveals that SAM tends to miss larger masks and erroneously categorise areas with unclear boundaries. In contrast, Uni-OVSeg demonstrates exceptional precision in segmenting objects of varying scales and different stuff. More experimental results are visualisation can be found in the Appendix B and C.

4.3. Ablation study

We conduct an extensive ablation study to demonstrate the contribution of each component of our framework.

Mask-text alignment. Compared to the straightforward baseline, as shown in Tab. 3, our proposed Uni-OVSeg achieves significant gains of 4.8% PQ and 9.5% mIoU on the COCO dataset, and 11.2% mIoU on the PASCAL

Context-59 dataset. This demonstrates our method effectively align objects in images and entities in text descriptions, generalising the CLIP embedding space from the image level to pixel level. By resorting to the refinement of text descriptions, new texts are more correlated with the corresponding images, improving the mIoU from 34.5% to 37.3% on the COCO dataset. Compared to the traditional NLP toolkit (NLTK) [3], ChatGPT-based parser extracts more reliable entities from text descriptions, which achieves obvious improvements of 3.1% and 3.7% mIoU on the COCO and PASCAL Context-59 datasets, respectively. Finally, the proposed multi-scale ensemble strategy that leverages the multi-scale information of objects within the images, stabilise the mask-text matching, which achieves a performance gain of 1.8% PQ on the COCO datasets.

Multi-scale ensemble in mask-text matching. The quality of correspondence between masks and entities is an essential part of mask-text matching. To investigate the impact of multi-scale information on this correspondence, as illustrated in Tab. 4, we use masks and semantic classes from

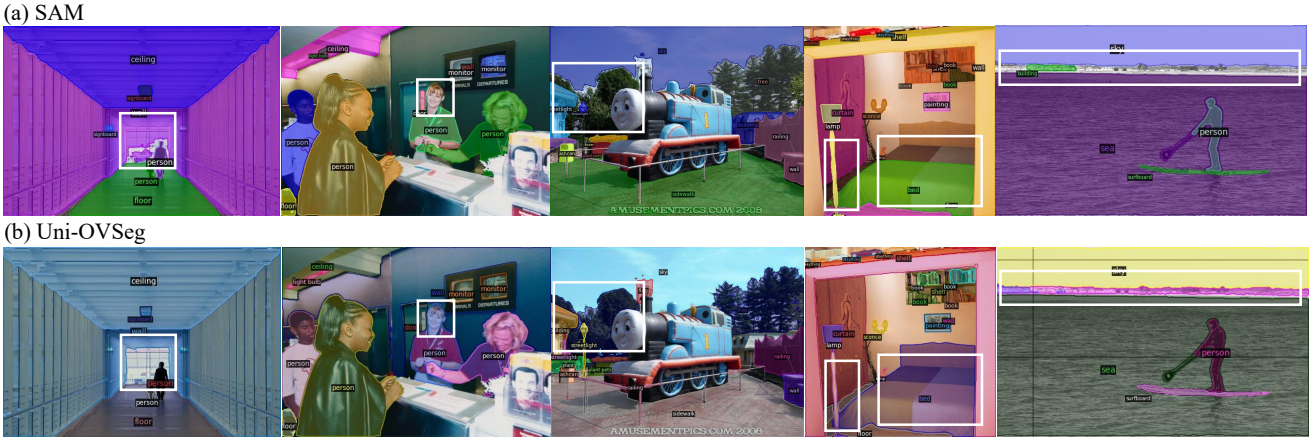


Figure 4. Visualisation of point-promptable automatic mask generation. We adopt a 20×20 point grid as a visual prompt and select the output masks with max IoU by calculating the IoU with the ground truth masks.

Table 3. **Ablation study on mask-text alignment.** “*Refine*.” denotes the text refinement by the LViM. “*Parser*.” denotes the text parser, which extracts entities from text descriptions. “NLTK” and “GPT” denote the natural language toolkit and ChatGPT-based parser. “*M.S.*” denotes the multi-scale ensemble strategy.

Refine. Parser. M.S.	COCO		PC-59
	PQ (%)	mIoU (%)	mIoU (%)
<i>baseline</i>	13.2	33.2	39.7
NLTK	14.1	34.5	40.9
✓ NLTK	15.6	37.3	44.5
✓ GPT	16.2	40.4	48.2
✓ GPT ✓	18.0	42.7	50.9

the ADE20K and COCO datasets, reporting the Top1 accuracy and forward time per sample. We first resize input images to multiple resolutions and extract visual features via the clip visual encoder. Given ground-truth masks, regional features are pooled from CLIP visual features and projected into the clip embedding space. Each regional embedding is classified by text embeddings. Taking into account the trade-off between performance and latency, we adopt the sizes of 869×896 and 1024×1024 as default.

5. Conclusion

In conclusion, this paper proposes an innovative framework for weakly-supervised open-vocabulary segmentation, named Uni-OVSeg. Using independent image-text and image-mask pairs, Uni-OVSeg effectively reduces the dependency on labour-intensive image-mask-text triplets, meanwhile achieving impressive segmentation performance in open-vocabulary settings. Using the LViM to refine text descriptions and multi-scale ensemble to enhance the quality of region embeddings, we alleviate the noise in mask-text correspondences, achieving substantial performance improvements. Notably, Uni-OVSeg significantly outper-

Table 4. **Mask classification performance.** we first pool the region features based on the provided ground truth masks. These pooled features are then projected into the CLIP embedding space, where they are classified using text embeddings. We report the Top-1 accuracy (%) and time (sec. / sample).

Input size	ADE20K	COCO	Time
768	45.2	49.0	0.10
896	48.3	53.4	0.13
1024	50.0	55.5	0.16
768, 896	49.2	55.2	0.20
896, 1024	51.3	58.3	0.26
768, 896, 1024	51.6	58.4	0.35

forms previous state-of-the-art weakly-supervised methods and even surpasses the cutting-edge fully-supervised method on the Challenging PASCAL Context-459 dataset. This impressive advancement demonstrates the superiority of our proposed framework and paves the way for further research.

6. Broader impacts

The Uni-OVSeg framework represents a significant advancement in open-vocabulary segmentation by reducing the dependency on labour-intensive image-mask-text triplet annotations. This innovation has the potential to democratise access to cutting-edge vision perception systems, offering substantial benefits across various sectors, such as medical imaging and autonomous vehicles. The development of a more efficient and accurate vision perception system contributes to the community, potentially leading to more innovative applications and research in machine learning, computer vision, and related areas. As with any AI model, there is a risk of bias in the data used for training. Efforts must be made to ensure that the datasets are diverse and representative to avoid perpetuating or amplifying biases.

References

[1] Jean-Baptiste Alayrac, Jeff Donahue, Pauline Luc, Antoine Miech, Iain Barr, Yana Hasson, Karel Lenc, Arthur Mensch, Katherine Millican, Malcolm Reynolds, et al. Flamingo: a visual language model for few-shot learning. *NeurIPS*, 35: 23716–23736, 2022. 2

[2] Yingbin Bai, Erkun Yang, Zhaoqing Wang, Yuxuan Du, Bo Han, Cheng Deng, Dadong Wang, and Tongliang Liu. Rsa: Reducing semantic shift from aggressive augmentations for self-supervised learning. *NeurIPS*, 35:21128–21141, 2022. 2

[3] Steven Bird, Ewan Klein, and Edward Loper. *Natural language processing with Python: analyzing text with the natural language toolkit.* ” O'Reilly Media, Inc.”, 2009. 7

[4] Daniel Bolya, Chong Zhou, Fanyi Xiao, and Yong Jae Lee. Yolact: Real-time instance segmentation. In *ICCV*, pages 9157–9166, 2019. 2

[5] Kaixin Cai, Pengzhen Ren, Yi Zhu, Hang Xu, Jianzhuang Liu, Changlin Li, Guangrun Wang, and Xiaodan Liang. Mixreorg: Cross-modal mixed patch reorganization is a good mask learner for open-world semantic segmentation. In *ICCV*, pages 1196–1205, 2023. 6

[6] Junbum Cha, Jonghwan Mun, and Byungseok Roh. Learning to generate text-grounded mask for open-world semantic segmentation from only image-text pairs. In *CVPR*, pages 11165–11174, 2023. 2, 6

[7] Kai Chen, Jiangmiao Pang, Jiaqi Wang, Yu Xiong, Xiaoxiao Li, Shuyang Sun, Wansen Feng, Ziwei Liu, Jianping Shi, Wanli Ouyang, et al. Hybrid task cascade for instance segmentation. In *CVPR*, pages 4974–4983, 2019. 2

[8] Lin Chen, Jisong Li, Xiaoyi Dong, Pan Zhang, Conghui He, Jiaqi Wang, Feng Zhao, and Dahua Lin. Sharegpt4v: Improving large multi-modal models with better captions. *arXiv preprint arXiv:2311.12793*, 2023. 5

[9] Ting Chen, Lala Li, Saurabh Saxena, Geoffrey Hinton, and David J Fleet. A generalist framework for panoptic segmentation of images and videos. In *ICCV*, pages 909–919, 2023. 2

[10] Xi Chen, Shuang Li, Ser-Nam Lim, Antonio Torralba, and Hengshuang Zhao. Open-vocabulary panoptic segmentation with embedding modulation. *ICCV*, 2023. 7

[11] Bowen Cheng, Maxwell D Collins, Yukun Zhu, Ting Liu, Thomas S Huang, Hartwig Adam, and Liang-Chieh Chen. Panoptic-deeplab: A simple, strong, and fast baseline for bottom-up panoptic segmentation. In *CVPR*, pages 12475–12485, 2020. 2

[12] Bowen Cheng, Alex Schwing, and Alexander Kirillov. Per-pixel classification is not all you need for semantic segmentation. In *NeurIPS*, pages 17864–17875, 2021. 2

[13] Bowen Cheng, Ishan Misra, Alexander G Schwing, Alexander Kirillov, and Rohit Girdhar. Masked-attention mask transformer for universal image segmentation. In *CVPR*, pages 1290–1299, 2022. 2, 3, 4, 5, 12

[14] Luca Ciampi, Carlos Santiago, João Paulo Costeira, Claudio Gennaro, and Giuseppe Amato. Domain adaptation for traffic density estimation. In *VISIGRAPP (5: VISAPP)*, pages 185–195, 2021. 15

[15] Marius Cordts, Mohamed Omran, Sebastian Ramos, Timo Rehfeld, Markus Enzweiler, Rodrigo Benenson, Uwe Franke, Stefan Roth, and Bernt Schiele. The cityscapes dataset for semantic urban scene understanding. In *CVPR*, pages 3213–3223, 2016. 5

[16] Jian Ding, Nan Xue, Gui-Song Xia, and Dengxin Dai. Decoupling zero-shot semantic segmentation. In *CVPR*, pages 11583–11592, 2022. 2, 6

[17] Zheng Ding, Jieke Wang, and Zhuowen Tu. Open-vocabulary universal image segmentation with maskclip. 2023. 3, 6, 7

[18] Mark Everingham, Luc Van Gool, Christopher KI Williams, John Winn, and Andrew Zisserman. The pascal visual object classes (voc) challenge. *International Journal of Computer Vision*, 88:303–338, 2010. 5

[19] Jean-Michel Fortin, Olivier Gamache, Vincent Grondin, François Pomerleau, and Philippe Giguère. Instance segmentation for autonomous log grasping in forestry operations. In *2022 IEEE/RSJ International Conference on Intelligent Robots and Systems (IROS)*, pages 6064–6071. IEEE, 2022. 15

[20] Jun Fu, Jing Liu, Haijie Tian, Yong Li, Yongjun Bao, Zhiwei Fang, and Hanqing Lu. Dual attention network for scene segmentation. In *CVPR*, pages 3146–3154, 2019. 2

[21] Golnaz Ghiasi, Xiuye Gu, Yin Cui, and Tsung-Yi Lin. Scaling open-vocabulary image segmentation with image-level labels. In *ECCV*, pages 540–557, 2022. 3, 5, 6

[22] Xiuye Gu, Tsung-Yi Lin, Weicheng Kuo, and Yin Cui. Open-vocabulary object detection via vision and language knowledge distillation. *arXiv preprint arXiv:2104.13921*, 2021. 5

[23] Kaiming He, Georgia Gkioxari, Piotr Dollár, and Ross Girshick. Mask r-cnn. In *ICCV*, pages 2961–2969, 2017. 2, 3

[24] Kaiming He, Haoqi Fan, Yuxin Wu, Saining Xie, and Ross Girshick. Momentum contrast for unsupervised visual representation learning. In *CVPR*, pages 9729–9738, 2020. 2

[25] Kaiming He, Xinlei Chen, Saining Xie, Yanghao Li, Piotr Dollár, and Ross Girshick. Masked autoencoders are scalable vision learners. In *CVPR*, pages 16000–16009, 2022. 2

[26] Jungseok Hong, Michael Fulton, and Junaed Sattar. Trashcan: A semantically-segmented dataset towards visual detection of marine debris. *arXiv preprint arXiv:2007.08097*, 2020. 15

[27] Edward J Hu, Yelong Shen, Phillip Wallis, Zeyuan Allen-Zhu, Yuanzhi Li, Shean Wang, Lu Wang, and Weizhu Chen. Lora: Low-rank adaptation of large language models. *arXiv preprint arXiv:2106.09685*, 2021. 13

[28] Yixiang Huang, Zhaoqing Wang, Xin Jiang, Ming Wu, Chuang Zhang, and Jun Guo. Pointshift: Point-wise shift mlp for pixel-level cloud type classification in meteorological satellite imagery. In *IGARSS*, pages 607–610. IEEE, 2022. 2

[29] Gabriel Ilharco, Mitchell Wortsman, Ross Wightman, Cade Gordon, Nicholas Carlini, Rohan Taori, Achal Dave, Vaishaal Shankar, Hongseok Namkoong, John Miller, Hanneh Hajishirzi, Ali Farhadi, and Ludwig Schmidt. Open-

clip, 2021. If you use this software, please cite it as below.
 5

[30] Chao Jia, Yinfai Yang, Ye Xia, Yi-Ting Chen, Zarana Parekh, Hieu Pham, Quoc Le, Yun-Hsuan Sung, Zhen Li, and Tom Duerig. Scaling up visual and vision-language representation learning with noisy text supervision. In *ICML*, pages 4904–4916, 2021. 2, 3

[31] Richard M Karp, Umesh V Vazirani, and Vijay V Vazirani. An optimal algorithm for on-line bipartite matching. In *STOC*, pages 352–358, 1990. 5

[32] Diederik P Kingma and Jimmy Ba. Adam: A method for stochastic optimization. *arXiv preprint arXiv:1412.6980*, 2014. 5

[33] Alexander Kirillov, Kaiming He, Ross Girshick, Carsten Rother, and Piotr Dollár. Panoptic segmentation. In *CVPR*, pages 9404–9413, 2019. 2, 3

[34] Alexander Kirillov, Eric Mintun, Nikhila Ravi, Hanzi Mao, Chloe Rolland, Laura Gustafson, Tete Xiao, Spencer Whitehead, Alexander C Berg, Wan-Yen Lo, et al. Segment anything. *ICCV*, 2023. 2, 3, 4, 5, 7, 14

[35] Boyi Li, Kilian Q Weinberger, Serge Belongie, Vladlen Koltun, and Rene Ranftl. Language-driven semantic segmentation. In *ICLR*, 2022. 2, 6

[36] Feng Li, Hao Zhang, Peize Sun, Xueyan Zou, Shilong Liu, Jianwei Yang, Chunyuan Li, Lei Zhang, and Jianfeng Gao. Semantic-sam: Segment and recognize anything at any granularity. *arXiv preprint arXiv:2307.04767*, 2023. 3

[37] Zhiqi Li, Wenhui Wang, Enze Xie, Zhiding Yu, Anima Anandkumar, Jose M Alvarez, Ping Luo, and Tong Lu. Panoptic segformer: Delving deeper into panoptic segmentation with transformers. In *CVPR*, pages 1280–1289, 2022. 5

[38] Chen Liang, Wenguan Wang, Jiaxu Miao, and Yi Yang. Gmmseg: Gaussian mixture based generative semantic segmentation models. In *NeurIPS*, pages 31360–31375, 2022. 2

[39] Feng Liang, Bichen Wu, Xiaoliang Dai, Kunpeng Li, Yinan Zhao, Hang Zhang, Peizhao Zhang, Peter Vajda, and Diana Marculescu. Open-vocabulary semantic segmentation with mask-adapted clip. In *CVPR*, pages 7061–7070, 2023. 2, 6

[40] Tsung-Yi Lin, Michael Maire, Serge Belongie, James Hays, Pietro Perona, Deva Ramanan, Piotr Dollár, and C Lawrence Zitnick. Microsoft coco: Common objects in context. In *ECCV*, pages 740–755, 2014. 5, 15

[41] Tsung-Yi Lin, Piotr Dollár, Ross Girshick, Kaiming He, Bharath Hariharan, and Serge Belongie. Feature pyramid networks for object detection. In *CVPR*, pages 2117–2125, 2017. 12

[42] Haotian Liu, Chunyuan Li, Qingyang Wu, and Yong Jae Lee. Visual instruction tuning. *arXiv preprint arXiv:2304.08485*, 2023. 2, 5

[43] Zhuang Liu, Hanzi Mao, Chao-Yuan Wu, Christoph Feichtenhofer, Trevor Darrell, and Saining Xie. A convnet for the 2020s. In *CVPR*, pages 11976–11986, 2022. 5

[44] Jonathan Long, Evan Shelhamer, and Trevor Darrell. Fully convolutional networks for semantic segmentation. In *CVPR*, pages 3431–3440, 2015. 2, 3

[45] Ilya Loshchilov and Frank Hutter. Decoupled weight decay regularization. *arXiv preprint arXiv:1711.05101*, 2017. 5

[46] Huaishao Luo, Junwei Bao, Youzheng Wu, Xiaodong He, and Tianrui Li. Segclip: Patch aggregation with learnable centers for open-vocabulary semantic segmentation. In *ICML*, pages 23033–23044, 2023. 3, 6

[47] Dantong Niu, Xudong Wang, Xinyang Han, Long Lian, Roei Herzig, and Trevor Darrell. Unsupervised universal image segmentation. *arXiv preprint arXiv:2312.17243*, 2023. 7

[48] Alec Radford, Jong Wook Kim, Chris Hallacy, Aditya Ramesh, Gabriel Goh, Sandhini Agarwal, Girish Sastry, Amanda Askell, Pamela Mishkin, Jack Clark, et al. Learning transferable visual models from natural language supervision. In *ICML*, pages 8748–8763, 2021. 2, 3, 5

[49] Kanchana Ranasinghe, Brandon McKinzie, Sachin Ravi, Yinfai Yang, Alexander Toshev, and Jonathon Shlens. Perceptual grouping in contrastive vision-language models. In *ICCV*, pages 5571–5584, 2023. 6

[50] Piyush Sharma, Nan Ding, Sebastian Goodman, and Radu Soricut. Conceptual captions: A cleaned, hypernymed, image alt-text dataset for automatic image captioning. In *ACL*, pages 2556–2565, 2018. 2

[51] Corey Snyder and Minh Do. Streets: A novel camera network dataset for traffic flow. *NeurIPS*, 32, 2019. 15

[52] Bart Thomee, David A Shamma, Gerald Friedland, Benjamin Elizalde, Karl Ni, Douglas Poland, Damian Borth, and Li-Jia Li. Yfcc100m: The new data in multimedia research. *Communications of the ACM*, 59(2):64–73, 2016. 2

[53] Zhi Tian, Chunhua Shen, and Hao Chen. Conditional convolutions for instance segmentation. In *ECCV*, pages 282–298, 2020. 2

[54] Zhi Tian, Bowen Zhang, Hao Chen, and Chunhua Shen. Instance and panoptic segmentation using conditional convolutions. *IEEE Transactions on Pattern Analysis and Machine Intelligence*, 45(1):669–680, 2022. 2

[55] Ashish Vaswani, Noam Shazeer, Niki Parmar, Jakob Uszkoreit, Llion Jones, Aidan N Gomez, Łukasz Kaiser, and Illia Polosukhin. Attention is all you need. *NeurIPS*, 30, 2017. 3, 4

[56] Huiyu Wang, Yukun Zhu, Bradley Green, Hartwig Adam, Alan Yuille, and Liang-Chieh Chen. Axial-deeplab: Standalone axial-attention for panoptic segmentation. In *ECCV*, pages 108–126, 2020. 2

[57] Huiyu Wang, Yukun Zhu, Hartwig Adam, Alan Yuille, and Liang-Chieh Chen. Max-deeplab: End-to-end panoptic segmentation with mask transformers. In *CVPR*, pages 5463–5474, 2021. 2

[58] Haoxiang Wang, Pavan Kumar Anasosalu Vasu, Fartash Faghri, Raviteja Vemulapalli, Mehrdad Farajtabar, Sachin Mehta, Mohammad Rastegari, Oncel Tuzel, and Hadi Pouransari. Sam-clip: Merging vision foundation models towards semantic and spatial understanding. *arXiv preprint arXiv:2310.15308*, 2023. 6

[59] Xinlong Wang, Rufeng Zhang, Chunhua Shen, Tao Kong, and Lei Li. Solo: A simple framework for instance segmentation. *IEEE Transactions on Pattern Analysis and Machine Intelligence*, 44(11):8587–8601, 2021. 2

[60] Xudong Wang, Rohit Girdhar, Stella X Yu, and Ishan Misra. Cut and learn for unsupervised object detection and instance segmentation. In *CVPR*, pages 3124–3134, 2023. 7

[61] Zhaoqing Wang, Ziyu Chen, Yaqian Li, Yandong Guo, Jun Yu, Mingming Gong, and Tongliang Liu. Mosaic representation learning for self-supervised visual pre-training. In *ICLR*, 2022. 2

[62] Zhaoqing Wang, Qiang Li, Guoxin Zhang, Pengfei Wan, Wen Zheng, Nannan Wang, Mingming Gong, and Tongliang Liu. Exploring set similarity for dense self-supervised representation learning. In *CVPR*, pages 16590–16599, 2022. 2

[63] Zhaoqing Wang, Yu Lu, Qiang Li, Xunqiang Tao, Yandong Guo, Mingming Gong, and Tongliang Liu. Cris: Clip-driven referring image segmentation. In *CVPR*, pages 11686–11695, 2022. 2

[64] Jiarui Xu, Shalini De Mello, Sifei Liu, Wonmin Byeon, Thomas Breuel, Jan Kautz, and Xiaolong Wang. Groupvit: Semantic segmentation emerges from text supervision. In *CVPR*, pages 18134–18144, 2022. 2, 3, 6

[65] Jilan Xu, Junlin Hou, Yuejie Zhang, Rui Feng, Yi Wang, Yu Qiao, and Weidi Xie. Learning open-vocabulary semantic segmentation models from natural language supervision. In *CVPR*, pages 2935–2944, 2023. 2, 3, 6

[66] Jiarui Xu, Sifei Liu, Arash Vahdat, Wonmin Byeon, Xiaolong Wang, and Shalini De Mello. Open-vocabulary panoptic segmentation with text-to-image diffusion models. In *CVPR*, pages 2955–2966, 2023. 3, 5, 6, 7

[67] Mengde Xu, Zheng Zhang, Fangyun Wei, Yutong Lin, Yue Cao, Han Hu, and Xiang Bai. A simple baseline for open-vocabulary semantic segmentation with pre-trained vision-language model. In *ECCV*, pages 736–753, 2022. 2, 3, 6

[68] Mengde Xu, Zheng Zhang, Fangyun Wei, Han Hu, and Xiang Bai. Side adapter network for open-vocabulary semantic segmentation. In *CVPR*, pages 2945–2954, 2023. 3, 6

[69] Lei Yang, Yan Zi Wei, Yisheng He, Wei Sun, Zhenhang Huang, Haibin Huang, and Haoqiang Fan. ishape: A first step towards irregular shape instance segmentation. *arXiv preprint arXiv:2109.15068*, 2021. 15

[70] Shuo Yang, Peize Sun, Yi Jiang, Xiaobo Xia, Ruiheng Zhang, Zehuan Yuan, Changhu Wang, Ping Luo, and Min Xu. Objects in semantic topology. In *ICLR*, 2021. 2

[71] Senthil Yogamani, Ciarán Hughes, Jonathan Horgan, Ganesh Sistu, Padraig Varley, Derek O’Dea, Michal Uricár, Stefan Milz, Martin Simon, Karl Amende, et al. Woodscape: A multi-task, multi-camera fisheye dataset for autonomous driving. In *Proceedings of the IEEE/CVF International Conference on Computer Vision*, pages 9308–9318, 2019. 15

[72] Haoxuan You, Haotian Zhang, Zhe Gan, Xianzhi Du, Bowen Zhang, Zirui Wang, Liangliang Cao, Shih-Fu Chang, and Yinfei Yang. Ferret: Refer and ground anything anywhere at any granularity. *arXiv preprint arXiv:2310.07704*, 2023. 2

[73] Jiahui Yu, Zirui Wang, Vijay Vasudevan, Legg Yeung, Mojtaba Seyedhosseini, and Yonghui Wu. Coca: Contrastive captioners are image-text foundation models. *arXiv preprint arXiv:2205.01917*, 2022. 2

[74] Qihang Yu, Huiyu Wang, Dahun Kim, Siyuan Qiao, Maxwell Collins, Yukun Zhu, Hartwig Adam, Alan Yuille, and Liang-Chieh Chen. Cmt-deeplab: Clustering mask transformers for panoptic segmentation. In *CVPR*, pages 2560–2570, 2022. 2

[75] Qihang Yu, Huiyu Wang, Siyuan Qiao, Maxwell Collins, Yukun Zhu, Hartwig Adam, Alan Yuille, and Liang-Chieh Chen. k-means mask transformer. In *ECCV*, pages 288–307, 2022. 2

[76] Qihang Yu, Ju He, Xueqing Deng, Xiaohui Shen, and Liang-Chieh Chen. Convolutions die hard: Open-vocabulary segmentation with single frozen convolutional clip. *NeurIPS*, 2023. 2, 3, 5, 6, 7

[77] Yuhui Yuan, Lang Huang, Jianyuan Guo, Chao Zhang, Xilin Chen, and Jingdong Wang. Ocnet: Object context for semantic segmentation. *International Journal of Computer Vision*, 129(8):2375–2398, 2021. 2

[78] Bowen Zhang, Zhi Tian, Quan Tang, Xiangxiang Chu, Xiaolin Wei, Chunhua Shen, et al. Segvit: Semantic segmentation with plain vision transformers. In *NeurIPS*, pages 4971–4982, 2022. 2

[79] Hang Zhang, Kristin Dana, Jianping Shi, Zhongyue Zhang, Xiaogang Wang, Ambrish Tyagi, and Amit Agrawal. Context encoding for semantic segmentation. In *CVPR*, pages 7151–7160, 2018. 2

[80] Hao Zhang, Feng Li, Xueyan Zou, Shilong Liu, Chunyuan Li, Jianwei Yang, and Lei Zhang. A simple framework for open-vocabulary segmentation and detection. In *ICCV*, pages 1020–1031, 2023. 3, 6

[81] Lingzhi Zhang, Shenghao Zhou, Simon Stent, and Jianbo Shi. Fine-grained egocentric hand-object segmentation: Dataset, model, and applications. In *European Conference on Computer Vision*, pages 127–145. Springer, 2022. 15

[82] Libo Zhang, Lutao Jiang, Ruyi Ji, and Heng Fan. Pidray: A large-scale x-ray benchmark for real-world prohibited item detection. *International Journal of Computer Vision*, 131(12):3170–3192, 2023. 15

[83] Wenwei Zhang, Jiangmiao Pang, Kai Chen, and Chen Change Loy. K-net: Towards unified image segmentation. *NeurIPS*, 34:10326–10338, 2021. 2

[84] Bolei Zhou, Hang Zhao, Xavier Puig, Sanja Fidler, Adela Barriuso, and Antonio Torralba. Scene parsing through ade20k dataset. In *CVPR*, pages 633–641, 2017. 5, 15

[85] Chong Zhou, Chen Change Loy, and Bo Dai. Extract free dense labels from clip. In *ECCV*, pages 696–712, 2022. 3

[86] Xizhou Zhu, Weijie Su, Lewei Lu, Bin Li, Xiaogang Wang, and Jifeng Dai. Deformable detr: Deformable transformers for end-to-end object detection. In *ICLR*, 2020. 4

[87] Xueyan Zou, Zi-Yi Dou, Jianwei Yang, Zhe Gan, Linjie Li, Chunyuan Li, Xiyang Dai, Harkirat Behl, Jianfeng Wang, Lu Yuan, et al. Generalized decoding for pixel, image, and language. In *CVPR*, pages 15116–15127, 2023. 2, 6, 14, 15

[88] Xueyan Zou, Jianwei Yang, Hao Zhang, Feng Li, Linjie Li, Jianfeng Gao, and Yong Jae Lee. Segment everything everywhere all at once. *arXiv preprint arXiv:2304.06718*, 2023. 2

A. Framework details

Inputs. For input images, we initially apply a random horizontal flip to each image. Subsequently, the image is randomly scaled to a resolution within the range of 716×716 to 1075×1075 resolutions. Finally, a crop of 896×896 resolutions is extracted from the scaled image to serve as the input. Regarding the category names, we construct a sentence using a prompt and tokenise it using a lower-cased byte pair encoding (BPE). For the visual prompt, we create a uniform grid of points with dimensions $h \times w$, which is aligned with the center of the pixels.

CLIP encoder. In general, the CLIP encoder can be any architecture. Motivated by the scalability of different input resolutions, we employ a ConvNext-based CLIP model to serve as both the image and text encoders. The image encoder is configured as a ConvNext-Large model, comprising four stages. Each stage contains a different number of blocks: 3 in the first, 3 in the second, 27 in the third, and 3 in the fourth. In contrast, the text encoder is structured as a 16-layer transformer, each layer being 768 units wide and featuring 12 attention heads. We harness the power of multi-scale features extracted by the image encoder. These features are represented as feature maps of varying widths and scales: a 192-wide feature map downsampled by a factor of 4, a 384-wide map downsampled by 8, a 768-wide map downsampled by 16, and a 1536-wide map downsampled by 32.

Pixel decoder. Following Mask2Former [13], we incorporate a lightweight pixel decoder based on the widely used Feature Pyramid Network (FPN) architecture [41]. We first adopt a 6-layer multi-scale deformable transformer on the multi-scale features to aggregate contextual information. Afterward, we upscale the low-resolution feature map in the decoder by a factor of 2 and then combine it with the corresponding resolution feature map from the backbone, which has been projected to match channel dimensions. This projection is achieved through a 1×1 convolution layer, followed by Group Normalization (GroupNorm). Subsequently, the merged features undergo further processing with an additional 3×3 convolution layer, complemented by GroupNorm and ReLU activation. This procedure is applied iteratively, beginning with the $32 \times$ downsampled feature map, until we attain a final feature map that is $4 \times$ downsampled. To generate pixel-wise embeddings, a single 1×1 convolution layer is applied at the end. Throughout the pixel decoder, all feature maps maintain a consistent dimension of 256 channels.

Visual prompt encoder. We have two types of visual prompts, including points and bounding boxes. Each type of prompts is mapped to 256-wide embeddings as follows. A point is first converted into a small bounding box. We represent a bounding box by an embedding pair, including the sine position embedding of its top-left and bottom-right corners. Afterward, we use two extra learnable embeddings to indicate these two corners.

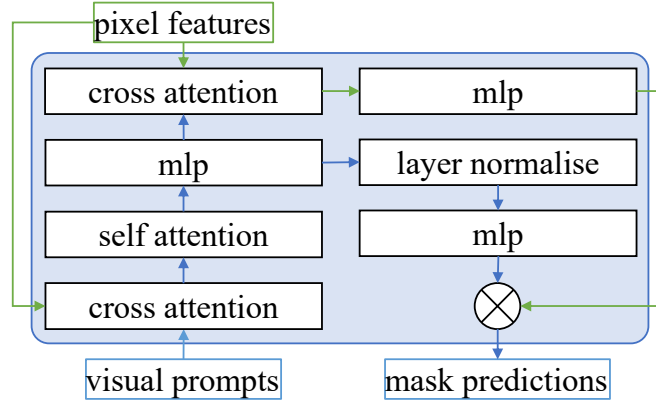


Figure 5. **Architecture of the mask decoder layer.** This decoder layer updates both visual prompt embeddings and pixel features by the cross-attention layers. The self-attention layer is used to update visual prompts. At each attention layer, positional encodings are added to the pixel features, and the entire original visual prompts (including position encoding) are added to the updated visual prompts.

Mask decoder. Following Mask2Former, we use a similar transformer decoder design. Each visual prompt embedding within our framework is coupled with a sine positional embedding. As depicted in Fig. 5, our approach utilizes six mask decoder layers, and we apply the same loss function after each layer. Moreover, every decoder layer includes a cross-attention

layer. This layer is crucial as it ensures that the final pixel features are enriched with essential geometric information, such as point coordinates and bounding boxes. Besides, in each decoder layer, we use a cross-attention layer, which ensures that the final pixel features have access to critical geometric information (e.g., point coordinates, and boxes). Finally, visual prompt embeddings are fed to a layer normalization, followed by processing through a multiple perception layer (MLP). These processed embeddings are then dot-producted with the pixel features, culminating in the generation of mask predictions.

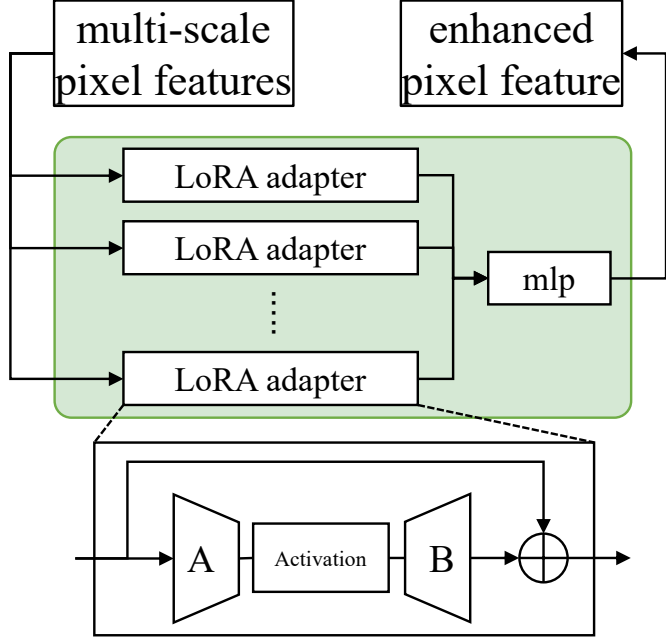


Figure 6. **Architecture of the multi-scale feature adapter.** Each LoRA adapter is used to update a specific downscaled features.

Multi-scale feature adapter. The multi-scale feature adapter illustrated in Fig. 6 is designed to refine and enhance pixel features at various scales. This adapter is composed of multiple Low-rank Adapters (LoRA adapters) [27], each specifically tailored to update features at a particular scale. Each LoRA adapter incorporates two linear layers, denoted as A and B, with a non-linear activation function placed in between. The linear layers A and B serve to transform the input data linearly, while the activation function introduces non-linearity, allowing for the modeling of more complex relationships in the data. Each adapter is responsible for handling features at a specific scale, suggesting a hierarchical approach to feature refinement. This modular design allows for a focused and specialized treatment of features depending on their resolution and semantic complexity, which can be particularly advantageous for dense prediction tasks.

B. Promptable segmentation.

Evaluation details. We perform a prompt segmentation evaluation on a wide range of datasets in various domains. For the point prompt, we adopt a uniform point grid $h \times w$ as input prompts (e.g., 20×20). For the box prompt, we use ground-truth bounding boxes as input prompts. 1-pt IoU denotes the oracle performance of one point by evaluating the intersection-over-union (IoU) of the predicted masks that best match ground truth. 1-box IoU denotes is similar to 1-pt IoU. More evaluation results are reported in Fig. 7, Fig. 8 and Fig. 9.

Dataset details. A description of each dataset is given in Tab. 5. The iShape dataset has 6 subsets, including antenna, branch, fence, hanger, log and wire.

C. Visualisation

We illustrate a wide range of visualisations of promptable segmentation and open-vocabulary segmentation across multiple datasets.

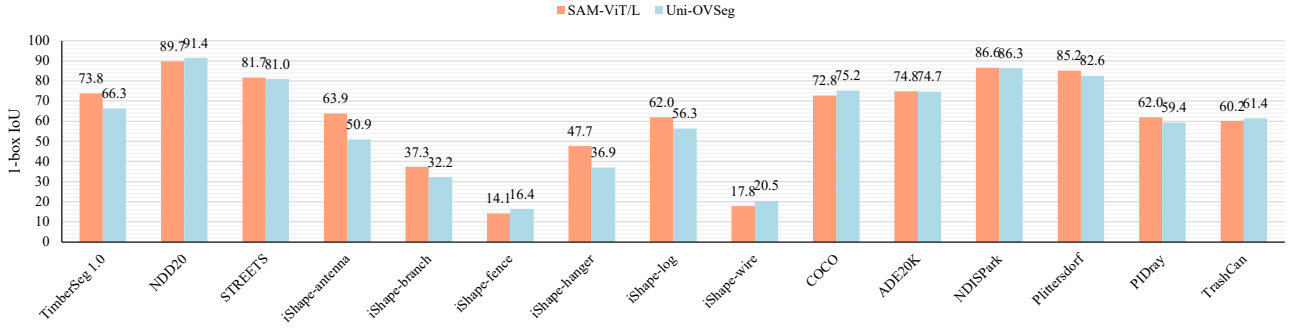


Figure 7. **Box-promptable segmentation performance.** We compare our method with SAM-ViT/L [34] on a wide range of datasets. Given a ground-truth box as the visual prompt, we select the output masks with max IoU by calculating the IoU with the ground-truth masks. We report 1-pt IoU for all datasets.

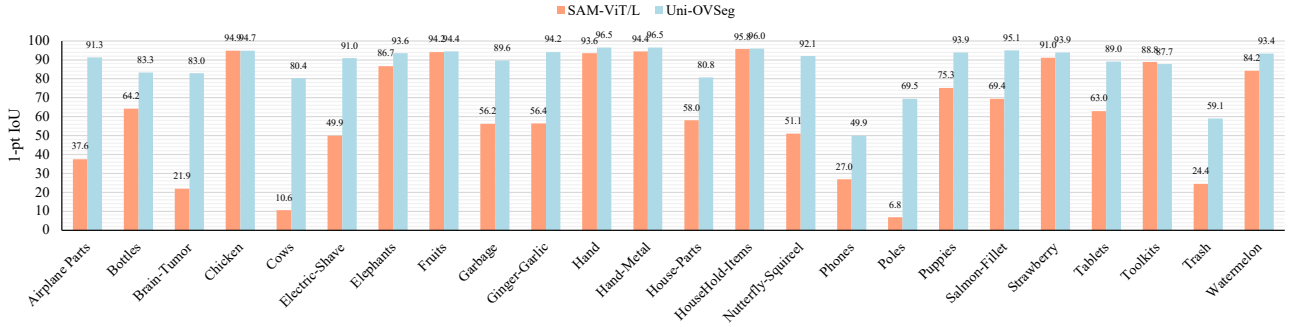


Figure 8. **Point-promptable segmentation performance.** We compare our method with SAM-ViT/L [34] on the SegInW datasets [87]. Given a 20×20 point grid as a visual prompt, we select the output masks with max IoU by calculating the IoU with the ground-truth masks. We report 1-pt IoU for all datasets.

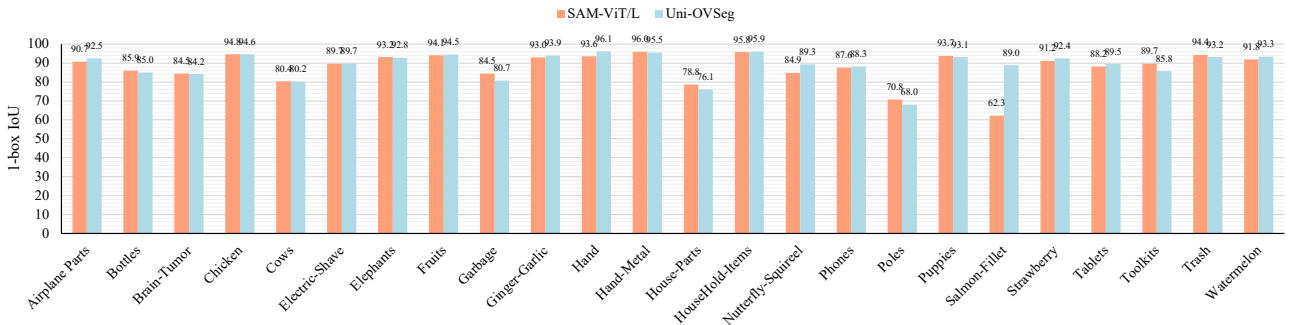


Figure 9. **Box-promptable segmentation performance.** We compare our method with SAM-ViT/L [34] on the SegInW datasets [87]. Given a ground-truth box as the visual prompt, we select the output masks with max IoU by calculating the IoU with the ground-truth masks. We report 1-pt IoU for all datasets.

Table 5. Segmentation datasets used to evaluate promptable segmentation with point and box prompts. The 11 datasets cover a broad range of domains, which are illustrated in “image type”.

Dataset	Image type	Mask type	Description
Egocentric Hand-Object Segmentation (EgoHOS) [81]	Egocentric	Instance	Fine-grained egocentric hand-object segmentation dataset. Dataset contains mask annotations for existing datasets.
TimberSeg 1.0 (TimberSeg) [19]	Logs	Instance	Segmentation masks of individual logs in piles of timber in various environments and conditions. Images are taken from an operator’s point-of-view.
STREETS [51]	Traffic camera	Instance	Segmentation masks of cars in traffic camera footage.
iShape [69]	Irregular shapes	Instance	Segmentation masks of irregular shapes like antennas, logs, shapes fences, and hangers.
COCO [40]	Scenes	Instance	Segmentation masks of complex everyday scenes containing common objects in their natural context.
ADE20K [84]	Scenes	Instance	Object and part segmentation masks for images from SUN and Places datasets.
Night and Day Instance Segmented Park (NDISPart) [14]	Parking lots	Instance	Images of parking lots from video footage taken at day and night during different weather conditions and camera angles for vehicle segmentation.
WoodScape [71]	Fisheye driving	Instance	Fisheye driving dataset with segmentation masks. Images are driving taken from four surround-view cameras.
PIDray [82]	X-ray	Instance	Segmentation masks of prohibited items in X-ray images of baggage.
TrashCan [26]	Underwater	Instance	Segmentation masks of trash in images taken by underwater ROVs. Images are sourced from the J-EDI dataset.
Segmentation in the wild (SegInW) [87]	Multiple domain	Instance	This dataset consists of 25 free public Segmentation datasets, crowd-sourced on roboflow.com .

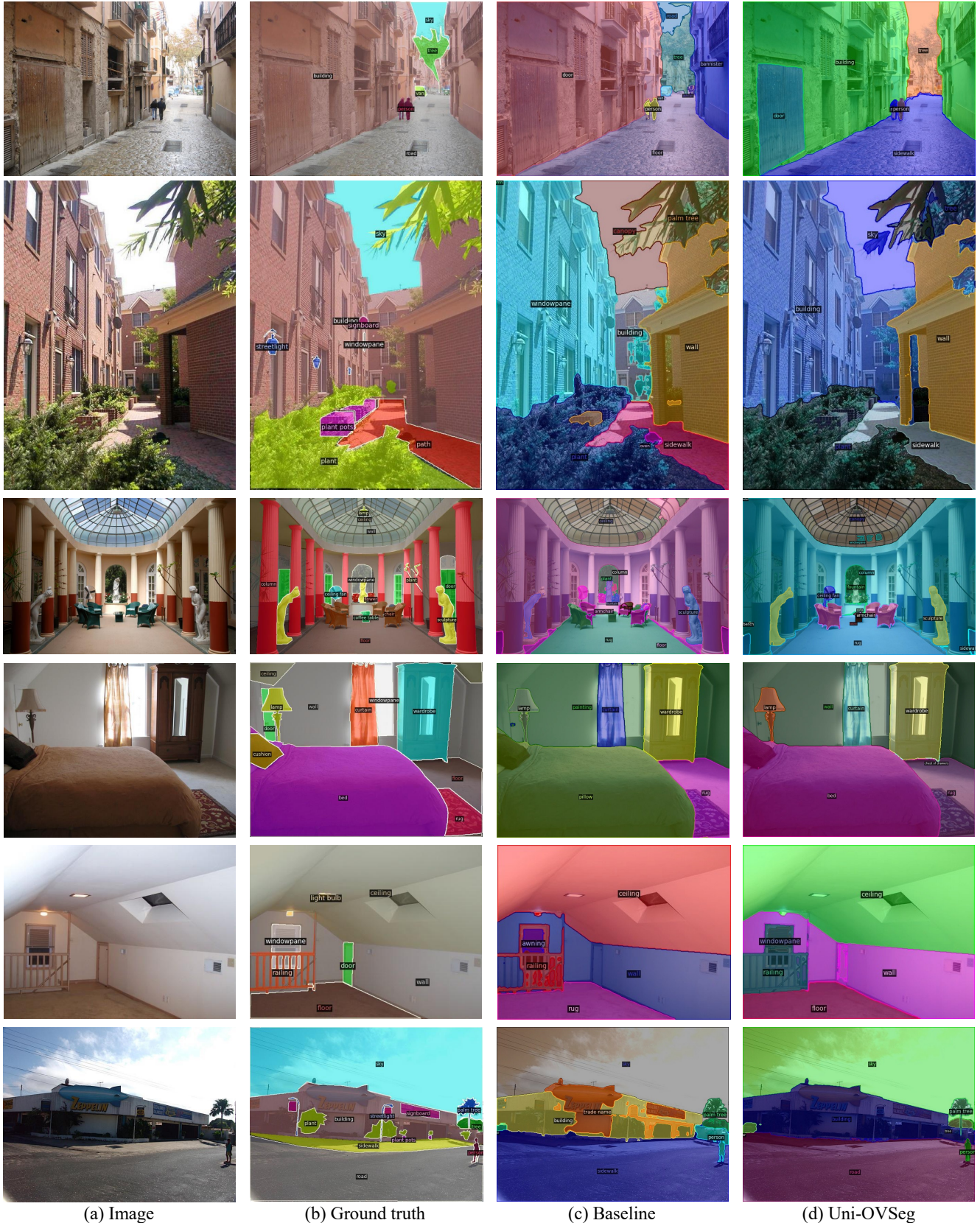


Figure 10. Visualisation of open-vocabulary segmentation between the baseline and ours Uni-OVSeg.



Figure 11. Visualisation of open-vocabulary segmentation between the baseline and ours Uni-OVSeg.

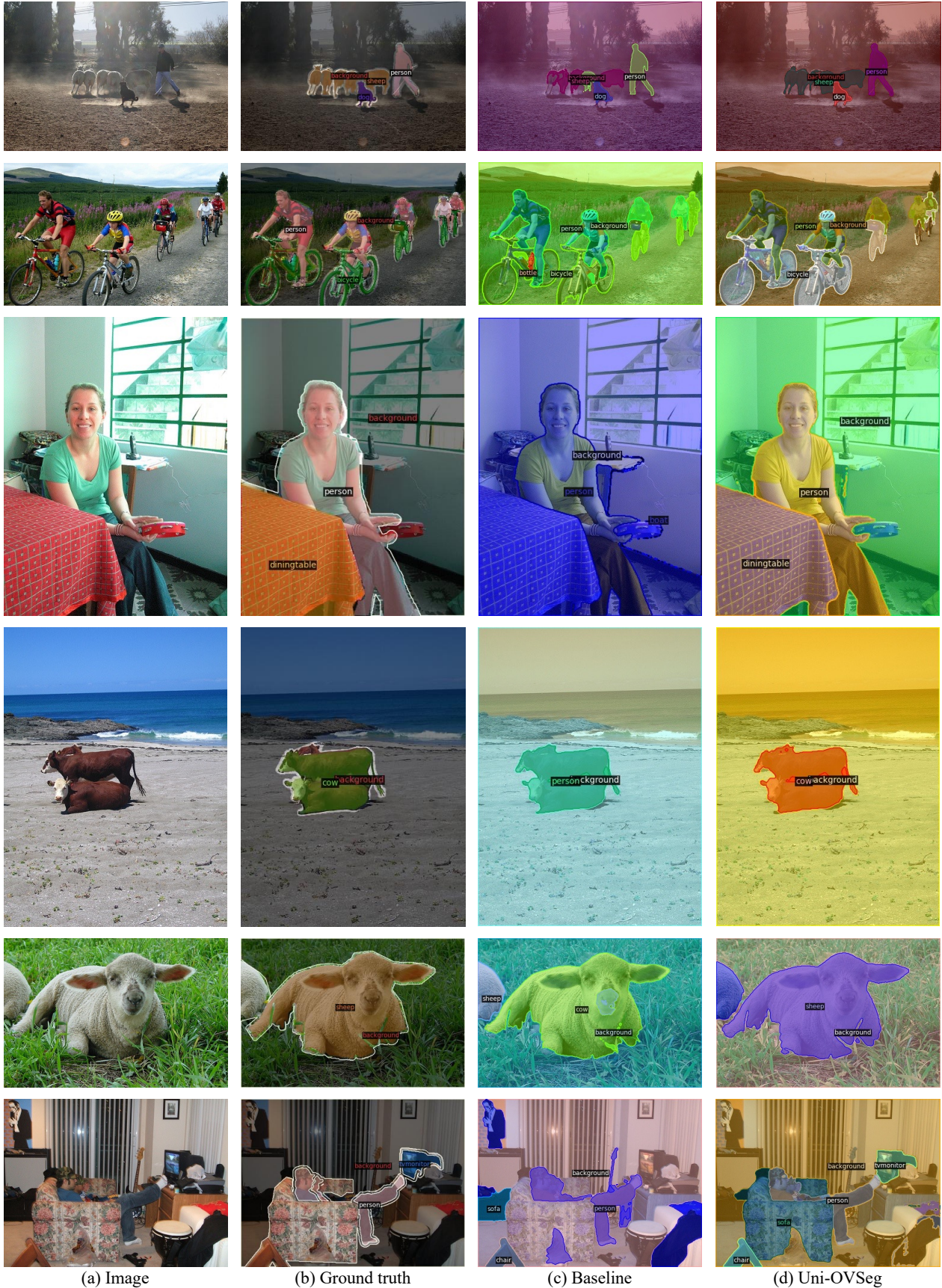
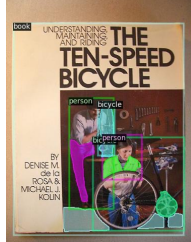
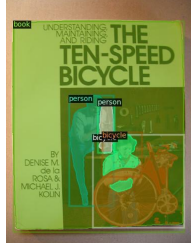


Figure 12. Visualisation of open-vocabulary segmentation between the baseline and ours Uni-OVSeg.

(a) SAM



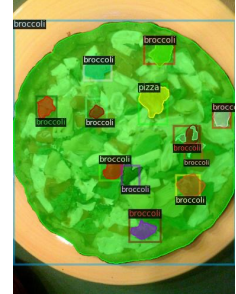
(b) Uni-OVSeg



(a) SAM



(b) Uni-OVSeg



(a) SAM



(b) Uni-OVSeg

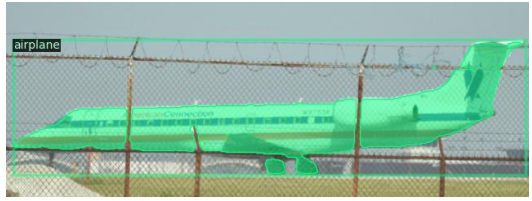


Figure 13. Visualisation of promptable segmentation between SAM-ViT/L and ours Uni-OVSeg.

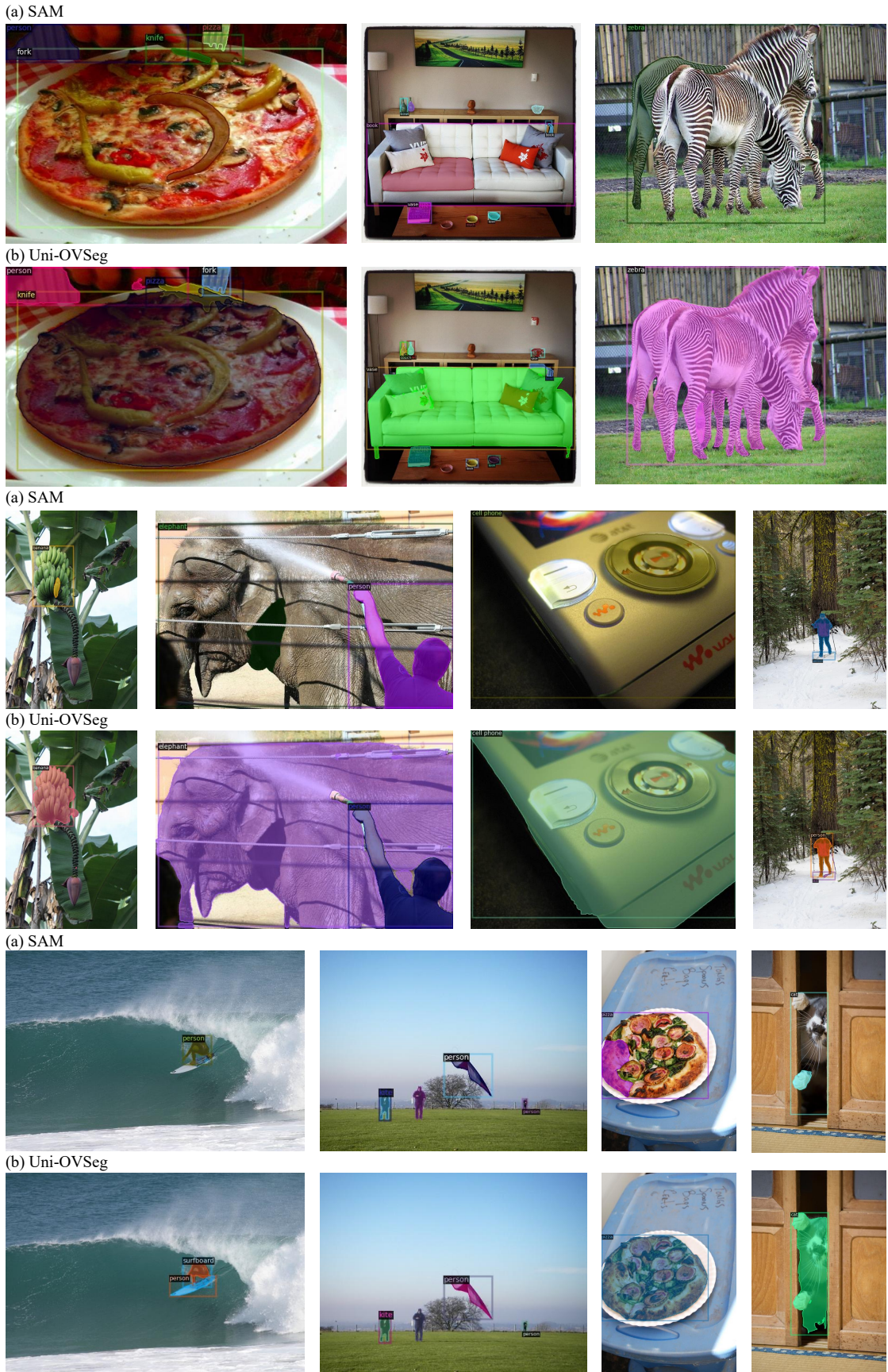


Figure 14. Visualisation of promptable segmentation between SAM-ViT/L and ours Uni-OVSeg.

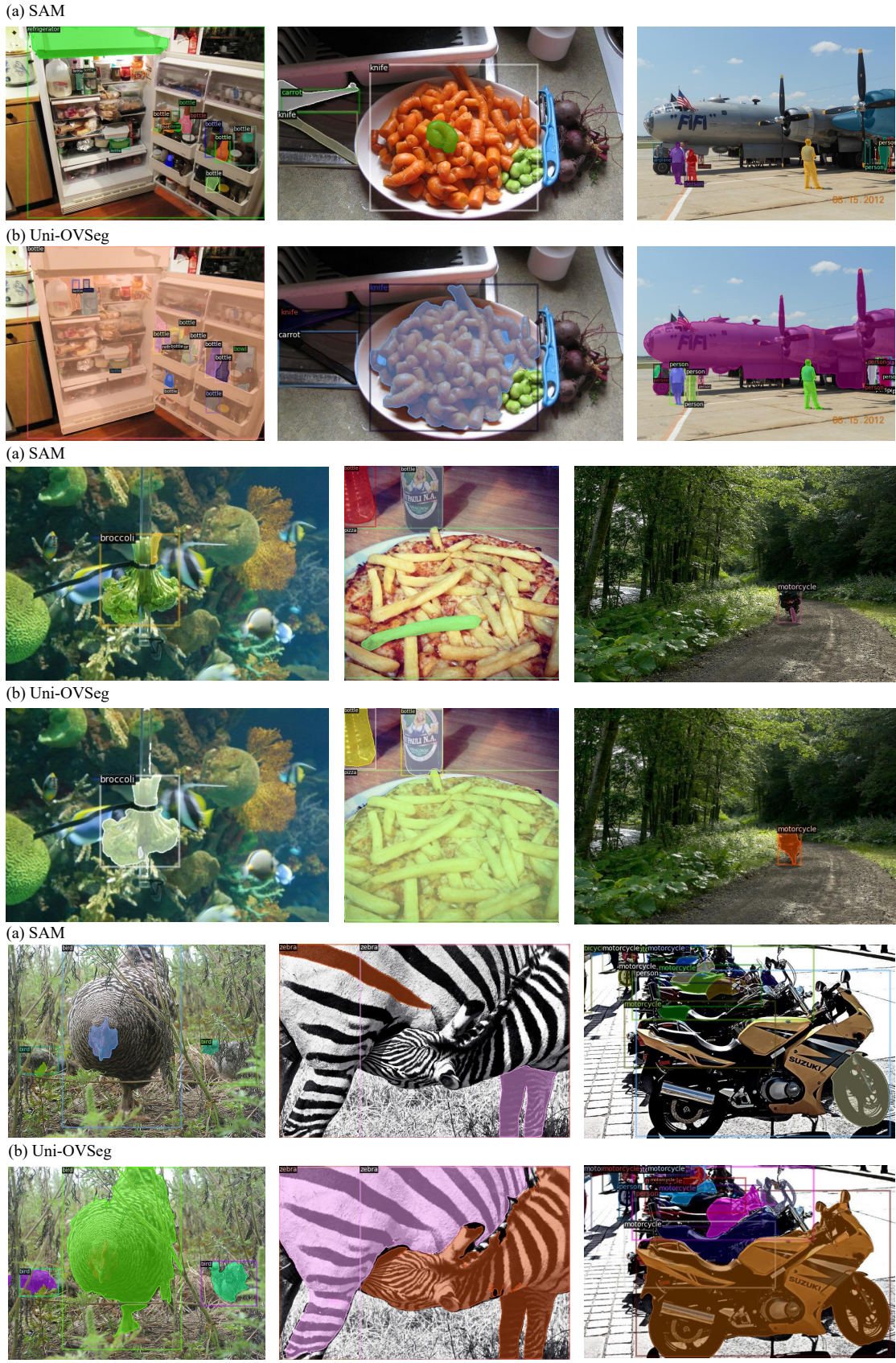


Figure 15. Visualisation of promptable segmentation between SAM-ViT/L and ours Uni-OVSeg.

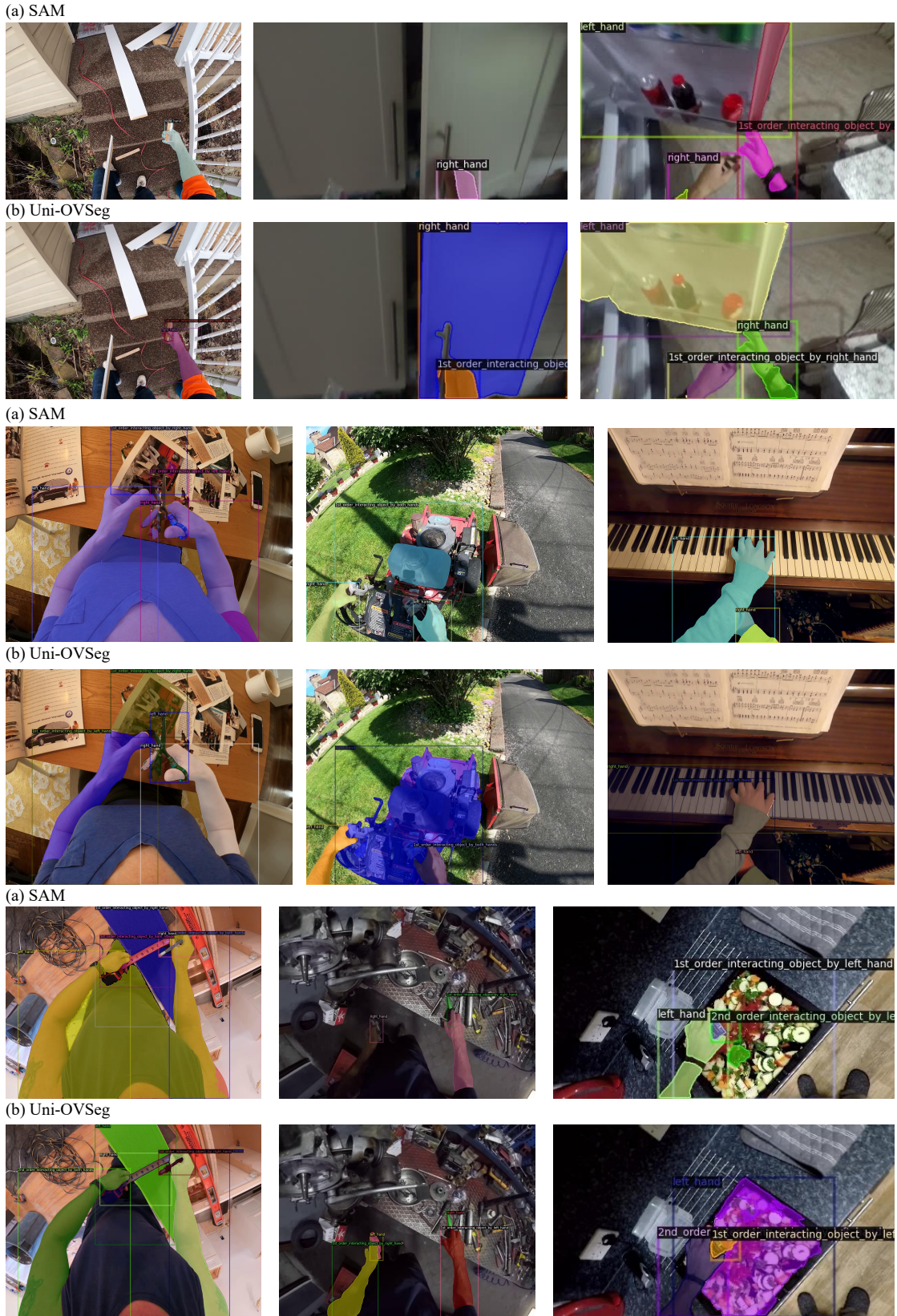


Figure 16. Visualisation of promptable segmentation between SAM-ViT/L and ours Uni-OVSeg.

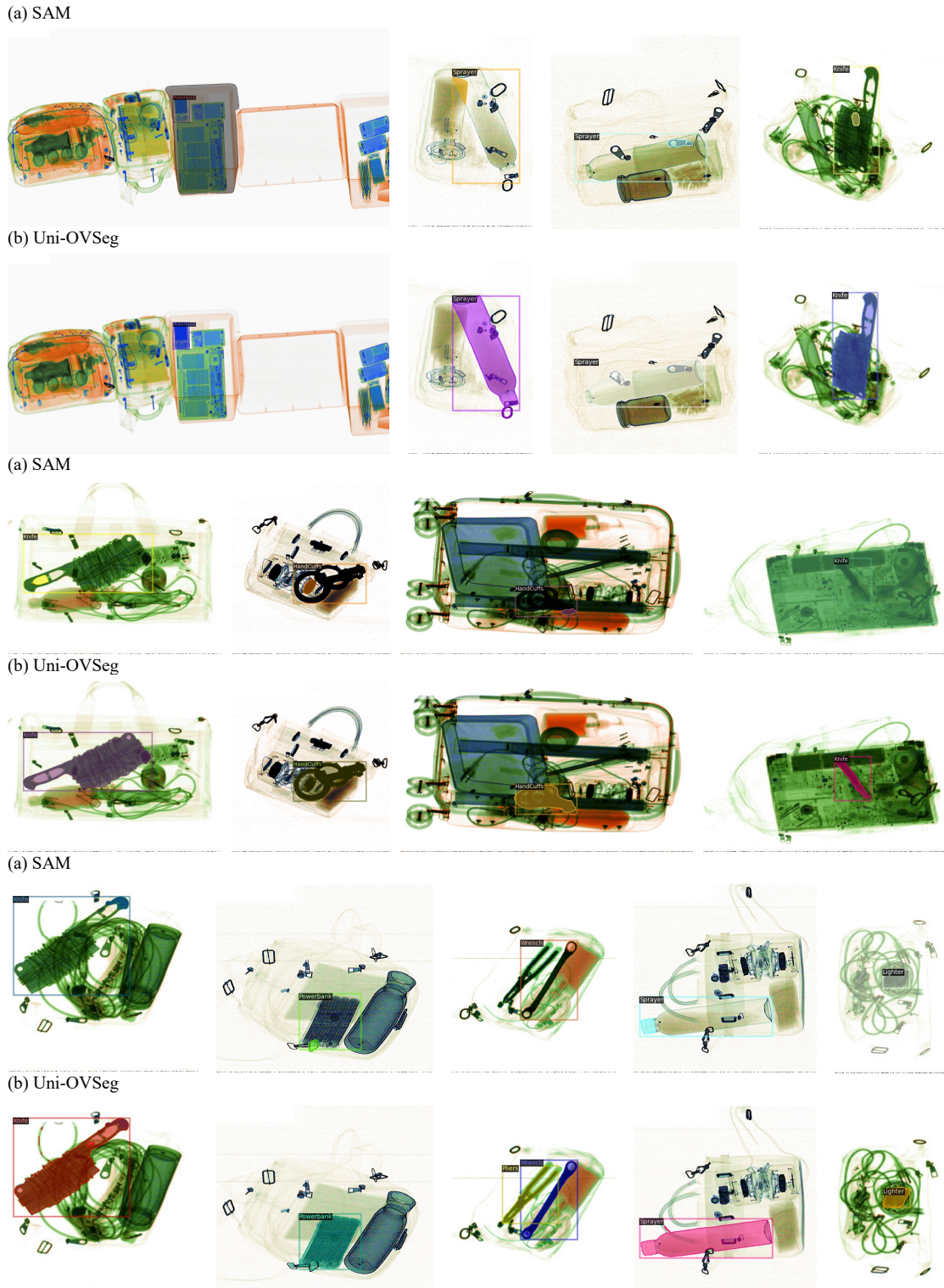


Figure 17. Visualisation of promptable segmentation between SAM-ViT/L and ours Uni-OVSeg.